# Nonlinear dendrites enable robust stimulus selectivity

Romain D. Cazé*, Sarah Jarvis, Simon R. Schultz

*Centre for Neurotechnology and Department of Bioengineering, Imperial College London, South Kensington, London, SW7 2AZ, UK*

* email: r.caze@imperial.ac.uk

August 2, 2015

**Hubel and Wiesel discovered that some neurons in the visual cortex (1) respond selectively to elongated visual stimuli of a particular orientation, proposing an elegant feedforward model to account for this selectivity. Since then, there has been much experimental support for this model, however several unexpected results, from *in vivo* two photon imaging of the dendrites of layer 2/3 pyramidal neurons in visual (2) and somatosensory (3) cortex cast doubt on the basic form of the model. Firstly, the dendrites may have different stimulus tuning to that of the soma. Secondly, hyperpolarizing a cell can result in it losing its stimulus selectivity, while the dendritic tuning remains unaffected. These results demonstrate the importance of dendrites in generating stimulus selectivity (4). Here, we implement stimulus selectivity in a biophysical model based on the realistic morphology of a layer 2/3 neuron, that can account for both of these experimental observations, within the feedforward framework motivated by Hubel and Wiesel. We show that this new model of stimulus selectivity is robust to the loss of synapses or dendrites, with stimulus selectivity maintained up to losses of 1/2 of the synapses, or 2/7 of the dendrites, demonstrating that in addition to increasing the computational capacity of neurons (5–8), dendrites also increase the robustness of neuronal computation. As well as explaining experimental results not predicted by Hubel and Wiesel, our study shows that dendrites enhance the resilience of cortical information processing, and prompts the development of new neuromorphic chips incorporating dendritic processing into their architecture.**

Over 50 years ago, Hubel and Wiesel discovered a canonical example of a neural computation (1), the responsivity of single neurons in the striate cortex to the orientation and direction of motion of a visual stimulus. The simple feed-forward model that they proposed to account for this has, although not without controversy, largely stood the test of time (see e.g. (9) for a review). Recently, however, two experimental groups provided strong evidence for the involvement of dendrites in processing orientation selectivity (2, 4). Using calcium imaging combined with a whole cell patch clamp to simultaneously monitor both somatic and dendritic activity, both groups found that activity in soma and dendrites can be activated separately. Although the soma reaches its maximal activity for a specific direction, they observed that some dendritic segments reach maximal activity for a variety of orientations different from the soma. Moreover, Jia et al. observed that hyperpolarization cancels somatic selectivity, while dendritic selectivity remains unaffected.

Dendrites enhance the computational capacity of single neurons. This stems from the local non-linear interaction of synaptic inputs in dendrites (10): the depolarization resulting from multiple synaptic inputs can be smaller (sublinear) or larger (supralinear) than their arithmetic sum. These non-linearities endow single neurons with greater computational capacity (6). We wanted to know here if such dendritic non-linearities might also explain the apparently counter-intuitive experimental observations described in the previous paragraph. For this purpose, we studied a possible implementation of direction and orientation selectivity, as a model of a more general canonical stimulus selectivity computation (3).

Synaptic integration depends on the rate and timing of presynaptic inputs. There is substantial evidence for encoding of stimulus information in correlations, beyond that present in firing rates (11, 12). Thus, we created input spike trains for which the presence of a stimulus (at all) increases the firing rate of all neurons, while the stimulus identity also increases correlation in a subset of neurons. Fig. 1A shows the activity of 400 presynaptic inputs divided in 8 groups of 50 inputs, in this model. The background firing rate of 1Hz increases to 10Hz during stimulus presentation for all neurons. In the subsets of 50 neurons encoding the stimulus identity, we added 20 synchronous events in which all neurons fire synchronously, raising the firing rate of this subset to 30 Hz.

Synaptic integration also depends on post-synaptic characteristics such as the neuronal morphology. We added AMPA/NMDA-type synapses at 7 distinct locations either scattered on 7 distinct primary dendrites or clustered on a single branch in a model neuron reconstructed from a layer 2/3 stellate cell (provided to us by Jia et al.) (Fig. 1B). Synaptic activation results in somatic depolarizations, the strength of which is independent of the distance of the synapse location to the soma, as observed in (13). We enforce this "dendritic democracy" (14) by scaling the synaptic conductance so that the resulting depolarization was 0.1 mV when measured at the soma (Fig. 1C). Interestingly, these synapses interact non-linearly in two distinct ways. When a low number of synapses activate simultaneously they can generate a depolarization larger than their arithmetic sum at the soma because of the voltage-gated magnesium block of the NMDA component (15)(Fig. 1C). In contrast, when more than 50 synapses activate within a small region (typically 50 $\mu$m), they interact sub-linearly. In this instance, the resulting voltage will be smaller than the expected arithmetic sum due to a smaller driving force (16, 17) (Fig. 1C black trace). In summary,

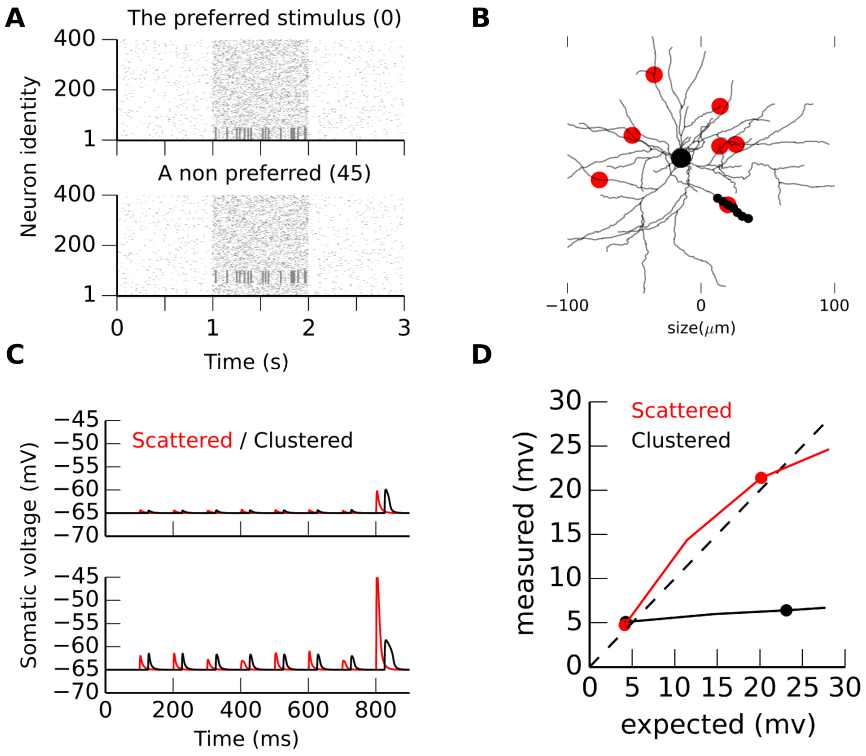


Figure 1: **Pre and post-synaptic characteristics enabling orientation selectivity A**. Scatter plot demonstrating the activity of the 400 presynaptic neurons during and outside a stimulation period (shaded area between 1 and 2s). When a stimulus is on the spiking probability goes from 0.01 to 0.1 in a 10ms window. The identity of the stimuli is encoded by multiple synchronous events (20 events) involving a particular group of neurons. **B** A reconstructed layer 2/3 neuron from (2). We base our passive biophysical model on this reconstruction. Dots are the 7 input sites in two situations (red:scattered/ black: clustered) **C** Somatic voltage trace when we stimulate a single input site (from 0 to 800ms) and when the seven input sites are stimulated simultaneously (800 to 1000ms). There are two traces, one where each site generate a 0.1mV at the soma (light) the other where we multiply the maximum conductance by five (dark). We do that for the two conditions (red:scattered/black:clustered) **D**. The expected/measured plot using the two stimulation protocols. The expected depolarization is the arithmetic sum of the individual depolarization. The measured depolarization is what is actually recorded in the model.

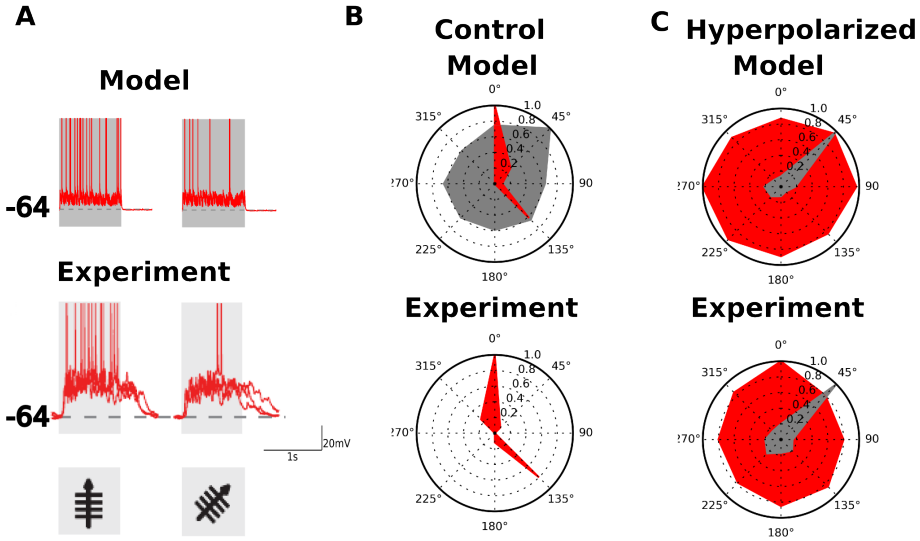


Figure 2: **Creating stimulus selectivity in silico A** The somatic voltage traces in response to two different stimuli (0/45 degrees). Top: model prediction ; bottom: experimental data). Both: horizontal line indicates resting potential (-64mV), and the gray shaded area indicates stimulus presentation. **B**. Polar plots describing the tuning of the soma (red) and of a dendrite (gray) which is the normalized spike count for soma or integral of the local membrane voltage. (top: model, bottom: experiment). **C**. As for **B**, but in which the neuron is hyperpolarized. Experimentally, hyperpolarization was induced by injecting $100pA$ to lower the threshold. From this, we calculated the tuning as the integral of the voltage. Similarly, we injected $100pA$. Experimental data replotted from (2) (Reproduce with permission of MacMillan publisher). (2).

all individual synapses create the same depolarization at the soma, respecting the so-called "synaptic democracy" (15), while multiple synapses can interact non-linearly depending on their location relative to each other.

This non-linear interaction between synapses makes the neuron sensitive to the spatial distribution of synaptic activity. To demonstrate this effect, we randomly selected two sets of 7 input sites located more than 60 $\mu$m from the soma, that were either clustered on a single dendrite or scattered on 7 different primary dendrites. The non-linear interaction between synapses depends on this distribution and on the input strength: for strong inputs, clustered synapses interact sub-linearly whereas scattered synapses interact almost linearly (Fig. 1D). This demonstrates that synaptic integration in a realistic reconstruction of a layer 2/3 spiny stellate cell is highly sensitive to the spatial distribution of active synapses, and even a small number of synapses can effectively depolarize the cell when active synapses are spatially dispersed throughout the dendrites.

We exploited this sensitivity to the spatial distribution of synapses to generate stimulus selectivity. In our implementation of stimuli selectivity, only the

neuronal population coding for the preferred stimulus synapse onto the 7 different primary dendritic branches, whereas the inputs coding for a non-preferred stimulus synapse onto a single dendritic branch. In this case, a single NMDA spike is generated and is, in most cases. insufficient to make the neuron spike. Conversely, for the preferred stimulus the neuron fires because multiple NMDA spikes are generated in parallel , as observed *in vivo* (18) (see Fig. 2.A). Both scenarios are clearly illustrated when viewed in real time (see movie S1 and S2).

Our implementation can reproduce the two counter-intuitive experimental observations: (i) that inputs from presynaptic neurons coding for the cell's preferred orientation do not clearly dominate (2, 4) (Fig. 2B), and (ii) that hyperpolarization disrupts the somatic but not the dendritic tuning (2) (Fig. 2C). As it linearizes integration in dendrites, hyperpolarization disturbs the selectivity of our *in silico* implementation. Conversely, dendritic selectivities become sharper because hyperpolarization increases the driving force at the input sites. In this implementation, the preferred stimulus activates the same number of synapses as the other stimuli. Thus, dendritic and somatic selectivity can differ. Jia et al. use the integral of the calcium concentration at distinct dendritic locations ("calcium hotspots") that were used as a proxy for the local voltage. With our model, we could directly measure the integral of the voltage signal at the input sites. In both cases, it is clear that activity in the soma and at one dendritic inputs site can be different (Fig. 3B).

Our implementation, reproducing the experimental data, is possible only if integration is locally non-linear and impossible if integration is linear. In both case, the transformation from input to output defines a set of inequalities. In the case of a stimuli selective neuron, the depolarization generated by the preferred stimuli should be higher than the action potential threshold, whereas the depolarization generated by a non-preferred stimulus should be lower than this threshold. If integration is linear it necessarily means that the preferred stimulus makes the highest number of synaptic contact. Conversely, if integration is locally non-linear the preferred stimulus can make a lower number of distributed contacts than the non-preferred stimuli. We formally demonstrate this result in the method section. It means that in our implementation the preferred stimulus can make the highest number of synapses but it is not a necessary condition anymore contrary to the case where integration is linear.

Next, we wanted to know if relaxing this necessity could add more robustness to our implementation. For that, we use an elementary model of synaptic integration to compute how the depolarization generated by a preferred or a non-preferred stimulus is distributed (Fig. 4). We scaled up our implementation to include 4900 synapses. There are 8 groups of presynaptic neurons and each group codes for a different stimulus. The group for preferred stimulus makes 700 synapses and the groups for the non-preferred stimuli each makes 650 synapses. Moreover, the group coding for the preferred stimulus targets all the dendrites randomly whereas the groups coding for the non-preferred stimuli have a tendency to cluster 30% of their synapses each on a different dendrite and the remaining synapses are distributed randomly. This slight bias in the spatial distribution of synapses is sufficient to clearly separate preferred from non-preferred inputs (Fig. 4A). To quantify the robustness of this model, we examined the effect of synapses or dendrites removal. We either randomly removed 2000 synapses or 2 dendritic subunits and compare at the effect on the ability to successfully discriminate whether the preferred or non-preferred stim-

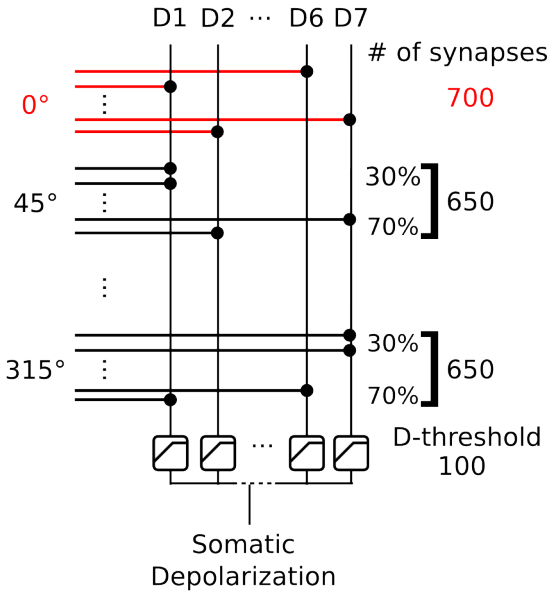


Figure 3: **Using the spatial distribution of synapses to implement stimulus selectivity.** Each horizontal line represents an axon coming from a presynaptic neuron. Red lines correspond to the population activated for the preferred stimulus. Each vertical line represents different dendrites or input sites. There are 8 groups of either 700 or 650 presynaptic neurons each making synapses (black circles) on one of the 7 dendritic subunits. The preferred stimulus makes 700 synapses randomly distributed. A non-preferred stimulus makes 650 and has a tendency to make contact on one input site (30% of synapses on this input site) distinct for each stimulus. A dendrite saturates when 100 synapses are active, in other words, the result of a dendritic filter cannot exceed 100. The somatic depolarization is the arithmetic sum of all the dendritic output.

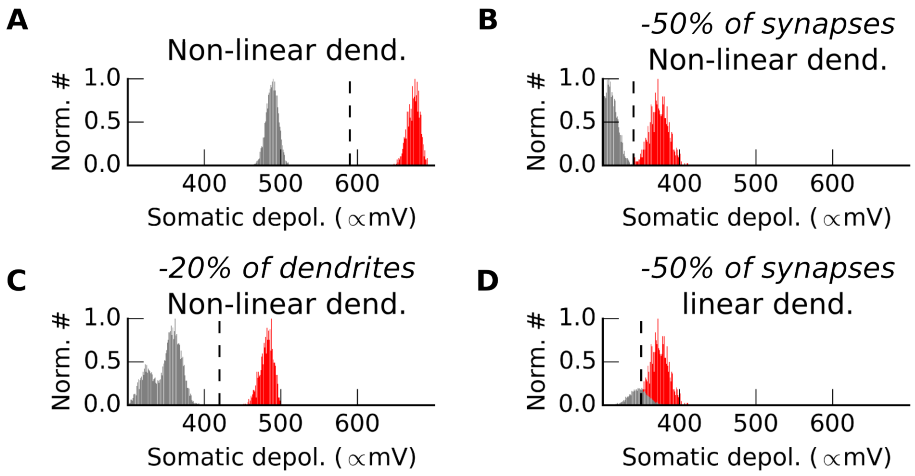


Figure 4: **Implementing stimulus selectivity robustly A**. We present 8 input patterns to 1000 random instances of our model and record the resulting somatic depolarization after the dendritic filtering for either a preferred (red) or the non-preferred (gray) input patterns. We count and normalize (Norm #) the number of input patterns generating a given somatic depolarization. It yields the distribution presented here for 8000 filtered input patterns. We present in **A** the case with non-linear dendrites that saturate at 100. If integration is linear you have two peaks one a 700 (preferred) and one at 650 (non-preferred). The vertical dotted line is a threshold that separates preferred from non-preferred inputs. **B**. We remove 50% if the synapses randomly and observe that the preferred and non-preferred stimuli are still easily separable (non-linear dendrites). **C**. We can even remove 20 % of dendrites and the neuron can still be selective after a recovery period (change in the somatic threshold). **D** In contrast, if we remove 50% of synapses in a linear model the two groups of pattern might be impossible to distinguish.

uli was presented (Fig. 4B and C). We observe that despite the loss of synapses, the two types of stimulus still generate clearly distinct soma depolarizations. This is similarly true when we removed 2 dendrites, and suggests that a neuron suffering synaptic or dendritic loss can sufficiently still be stimuli selective, to the degree that it should be possible to restore its spike threshold during a recovery period. If the preferred stimulus is not anymore the one with the highest number of synaptic contact then it becomes impossible for a model where integration is linear to be selective for this stimulus (Fig. 4D). It demonstrates that exploiting the spatial distribution of synapses enhances the robustness of the implementation to the loss of synapse or dendrites.

In summary, we demonstrated that non-linear summation enables neurons to implement robust stimuli selectivity. Our implementation explains how the neuron deals with the input coding for all the stimuli as observed by Jia et al. and Smith et al. (2, 4). It explains why hyperpolarizing the neuron could affect neuronal tuning as observed in (2, 3, 19). This implementation is also compatible with a bias in synaptic connectivity, where the strongest input comes from the preferred stimulus, as observed experimentally (20), further increasing the robustness. Finally, it predicts that a neuron can recover its tuning after losing a large fraction of either its synapses or dendrites.

Our results have strong follow-on implications for the design of neuromorphic chips, as they suggest that the implementation of dendritic compartments would not only increase the computational power of each unit, but also increase their resilience, addressing a crucial issue in the design of scalable and fault-tolerant neurocomputer architectures. While we have demonstrated these capabilities in the context of a neuron's selectivity to the orientation of a visual stimulus, the model we have proposed is general, and may reflect a canonical computational principle for stimulus selectivity.

# Method

## Biophysical model

The cable equations (21) are used to model how a depolarization propagates along the dendrites. The model was implemented using NEURON with Python to solve these equations (22). The axial resistance in all section is $R_a = 35.4\Omega$. This model contains only passive mechanism which correspond to constant current $i$ equal to $i_l = g_l \times (v(t) - e_t)$ with $g_l = 0.001\Omega^{-1}$, $v(t)$ the membrane voltage at time $t$ in $mV$ and $e_l = -65mV$.

The neuron model is spiking because of a hard threshold. When the somatic voltage reaches $-45mV$ we set the voltage of this section at $20mv$ at the next time step and then $-65mV$ as a reset potential.

## Conductance based NMDA-type synapses

The current generated by a synapse $i_s = g(t)g_{mg}(v) \times (v(t) - e_s)$ with g(t) a time dependent conductance depending on the presynaptic activity with an alpha function shape. It has two time constants for rise time $\tau_1 = 0.1ms$ and decay $\tau_2 = 10ms$, this time constant is lower than the real glutamate binding on NMDA channels time constant to account for the presence of voltage-gated

calcium dependent potassium channels in the membrane. The conductance $g_{mg}(v)$ depends on the voltage of the membrane and varies between 0.22 for $-65mV$ and 2 for $-8mV$. $v(t)$ is the current membrane voltage at time $t$ and $e_s = 0mV$ is the reversal potential for the channel. (see .mod file used to see a complete list of the used references).

### An abstract compartmental model

We used a model made using Python to compute synaptic integration. Each synapse $i$ makes a contact on the dendritic subunit $j$ so $w_{i,j} = 1$ or $w_{i,j} = 0$ it results in a local integration in the subunit $j$ equals to $d_j = \sum_i w_{i,j}$. This sum is then sub-linearly filtered: it cannot excess $\theta = 100$ to account for dendritic saturation. To obtain synaptic integration we sum all the $d_i$.

### Implementing our method in a linear model is impossible

Let us take the simplest situation with two presynaptic neurons each making a synaptic contact on a postsynaptic neuron. One of the presynaptic neuron code for the preferred direction and the other for a non-preferred direction. We write $W_{pref}$ the amplitude of the depolarization generated by the first neuron and $W_{non_pref}$ the one generated by the other neuron. A linear neuron implement direction selectivity only if $W_{pref} \geq \Theta$ and $W_{nonpref} < \Theta$ which is equivalent to $W_{pref} > \Theta > W_{nonpref}$. Therefore, direction selectivity necessary implies that the preferred direction has the highest weight. Note that this condition can be generalized to any number of presynaptic neurons, in this case the weights $W$ are the arithmetic sum of the individual depolarizations.

### Code availability

At the time of publication, the code used to generate the simulation and movies will be available on pip at neurhon15CaJaSc and also on Romain Cazé git repository: rcaze.

## Acknowledgments

Authors want to thank Dr. Andrew Gallimore for his comments. This work was supported by EU FP7 Marie Curie Initial Training Network 289146 NETT. SJ is supported by EU FP7 Marie Curie fellowship (PIEF-GA-2013-628086).

## References

[1] Hubel, D. H. & Wiesel, T. N. Receptive fields of single neurones in the cat's striate cortex. *The Journal of Physiology* **148**, 574–591 (1959).

[2] Jia, H., Rochefort, N. L., Chen, X. & Konnerth, A. Dendritic organization of sensory input to cortical neurons in vivo. *Nature* **464**, 1307–1312 (2010).

[3] Lavzin, M., Rapoport, S., Polsky, A., Garion, L. & Schiller, J. Nonlinear dendritic processing determines angular tuning of barrel cortex neurons in vivo. *Nature* **490**, 397–401 (2012).

[4] Smith, S. L., Smith, I. T., Branco, T. & Häusser, M. Dendritic spikes enhance stimulus selectivity in cortical neurons in vivo. *Nature* **503**, 115–20 (2013).

[5] Poirazi, P., Brannon, T. & Mel, B. Pyramidal neuron as two-layer neural network. *Neuron* **37**, 989–999 (2003).

[6] Cazé, R. D., Humphries, M. & Gutkin, B. Passive Dendrites Enable Single Neurons to Compute Linearly Non-separable Functions. *PLoS Computational Biology* **9** (2013).

[7] Cazé, R. D., Humphries, M. & Gutkin, B. S. Spiking and saturating dendrites differentially expand single neuron computation capacity. *Advances in neural information processing systems* **25**, 1–9 (2012).

[8] Zador, A. A. M., Claiborne, B., Brown, T. T. H. & Clairborne, B. J. Nonlinear pattern separation in single hippocampal neurons with active dendritic membrane. *Advances in neural information processing systems* 51–51 (1993).

[9] Reid, R. C. & Alonso, J.-M. The processing and encoding of information in the visual cortex (1996).

[10] Polsky, A., Mel, B. W. & Schiller, J. Computational subunits in thin dendrites of pyramidal cells. *Nature Neuroscience* **7**, 621–627 (2004).

[11] DeCharms, R. C. & Merzenich, M. M. Primary cortical representation of sounds by the coordination of action-potential timing. *Nature* **381**, 610–613 (1996).

[12] Bruno, R. M. & Sakmann, B. Cortex is driven by weak but synchronously active thalamocortical synapses. *Science* **312**, 1622–7 (2006).

[13] Smith, M., Ellis-Davies, G. & Magee, J. Mechanism of the distance-dependent scaling of Schaffer collateral synapses in rat CA1 pyramidal neurons. *The Journal of Physiology* **548**, 245 (2003).

[14] Häusser, M. Synaptic function: Dendritic democracy. *Current Biology* **11**, R10–R12 (2001).

[15] Nevian, T., Larkum, M., Polsky, A. & Schiller, J. Properties of basal dendrites of layer 5 pyramidal neurons: a direct patch-clamp recording study. *Nature* **200**, 7 (2007).

[16] Koch, C., Poggio, T. & Torres, V. Retinal ganglion cells: a functional interpretation of dendritic morphology. *Phil. Trans. R. So. Lond. B* **298**, 227–263 (1982).

[17] Tran-van Minh, A. *et al.* Contribution of sublinear and supralinear dendritic integration to neuronal computations. *Frontiers in Cellular Neuroscience* **9**, 1–15 (2015).

[18] Hill, D. N., Varga, Z., Jia, H., Sakmann, B. & Konnerth, A. Multibranch activity in basal and tuft dendrites during firing of layer 5 cortical neurons in vivo. *Proceedings of the National Academy of Sciences* **110**, 13618–13623 (2013).

[19] Lee, D., Lin, B.-J. & Lee, A. K. Hippocampal place fields emerge upon single-cell manipulation of excitability during behavior. *Science* **337**, 849–53 (2012).

[20] Chen, T.-W. *et al.* Ultrasensitive fluorescent proteins for imaging neuronal activity. *Nature* **499**, 295–300 (2013).

[21] Rall, W. Distinguishing theoretical synaptic potentials computed for different soma-dendritic distributions of synaptic input. *Journal of Neurophysiology* **30**, 1138–1168 (1967).

[22] Hines, M. L., Davison, A. P. & Muller, E. NEURON and Python. *Frontiers in Neuroinformatics* **3**, 1 (2009).